Optical Temperature Field Measurements with Two-Color Laser Induced Fluorescence in a Stratified Thermal Energy Storage

C. Naumann*, C. Cierpka

Department of Mechanical Engineering, Technische Universität Ilmenau, Germany
*Corresponding author: clemens.naumann@tu-ilmenau.de

Keywords: Laser induced fluorescence, Temperature field measurement, Thermal energy storage.

ABSTRACT

Thermal energy storage systems (TES) are an important part for storing surplus electric energy from renewable, volatile energy sources. TES using liquid storage materials operate most efficiently by stratifying the storage fluid based on its thermal density gradient into a hot and cold layer, separated by a thermocline region. Previous studies of such stratified TES have shown that heat conduction from the hot, upper layer to the cold, lower layer through the storage tank wall induces counter-directed convective flows (wall jets) along the inner walls. These wall jets carry hot fluid from the upper layer and cold fluid from the lower layer towards the thermocline region, which leads to mixing of the layers and therefore to a decreased thermal efficiency. To quantify the influence of the wall jets on the mixing process, optical temperature field measurements in the thermocline region of a $105\,\mathrm{L}$ stratified TES model experiment are performed with two-color planar laser induced fluorescence (2C-PLIF). The results show that the method is feasible for evaluating the thermocline temperature distribution over time in such a system with an accuracy of $1.5\,^{\circ}\mathrm{C}$. Further measurements in the hot wall jet region show that the temperature resolution of the measurement system limits the evaluation of the thermal boundary layers. However, the 2C-PLIF system provides sufficient temperature field information to determine the local heat fluxes in future studies in combination with simultaneous PIV measurements.

1. Introduction

Energy storage facilities are essential for storing surplus energy generated by volatile, renewable sources, ensuring a consistent and reliable energy supply while reducing the emissions of greenhouse gases. Thermal energy storage systems (TES) are used in Carnot batteries (Dumont et al. (2020)), where they can store large amounts of surplus electrical energy for long durations via power-to-heat-to-power coupling. A common type of TES is the stratified thermal energy storage, which utilizes the thermal density gradient of a liquid storage medium to create a stable stratification of hot fluid over cold fluid, separated by a thermocline region. To achieve optimum operation

conditions for such a storage type, it is not only important to minimize heat losses to the surrounding, but also to separate both fluid layers from each other. While heat losses to the environment lead to energy losses, which can be significantly reduced by efficient thermal insulation, mixing processes of both fluid layers lead to exergy destruction, which appears to be inherent for common stratified TES types - not only during charging and discharging processes, but also during standby periods. In fact, previous flow characterization studies in a model experiment for stratified TES with particle image velocimetry (PIV) (Otto & Cierpka (2021); Otto et al. (2023)) have shown that heat conduction from the hot, upper layer into the cold, lower layer through the storage tank wall leads to near-wall, counter-directed convective flows (wall jets), which transport hot fluid from the upper and cold fluid from the lower layer towards the thermocline region. This phenomenon, also called parasitic convection, is schematically shown in Figure 1 (left). The main reason for that

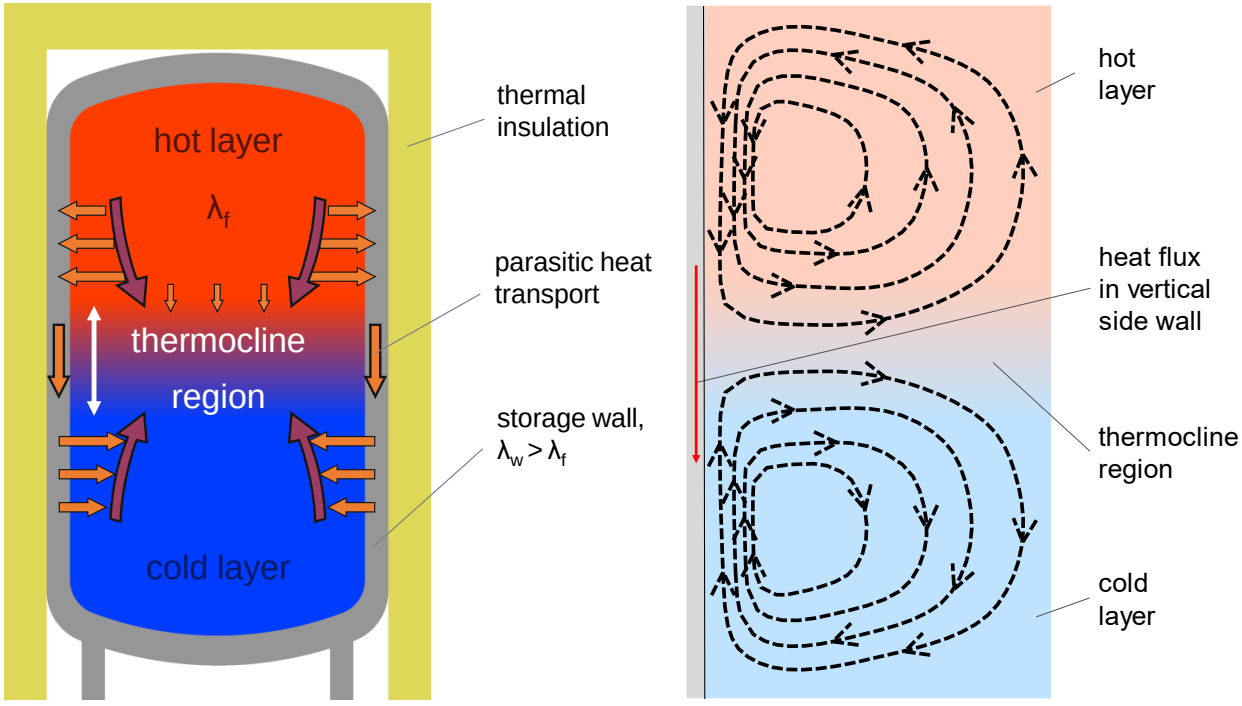

Figure 1. Left) Scheme of the phenomenon of parasitic convection inside a stratified TES; right) overall occuring flow structures inside a model experiment of a stratified TES.

is the high thermal conductivity of the wall compared to the storage medium, which results in a local temperature difference between wall and adjacent fluid, which in turn leads to the formation of a thermal boundary layer. This thermal boundary layer acts as the main driving force for these wall jets. Figure 1 (right) shows a schematic of the overall flow structures inside a stratified TES. Since mixing of the fluid layers reduces storage efficiency, it is important to quantify the influence of these convective flows on the inherent mixing process. For this reason, the present study is focusing on high-resolution optical temperature field measurements in the near wall thermocline region of a model experiment for stratified TES, using two-color planar laser induced fluorescence (2C-PLIF), complementary to previously performed PIV flow measurements.

2. Experimental Setup

The 2C-PLIF measurements are performed in a rectangular model experiment of a stratified TES made of transparent poly-carbonate with base dimensions of $375\,\mathrm{mm} \times 375\,\mathrm{mm}$ and a height of $750\,\mathrm{mm}$. This results in an overall fluid volume of $105\,\mathrm{L}$. An aluminum plate with a thickness of $10\,\mathrm{mm}$ is inserted into the model experiment at one side to mimic a real storage tank wall. For comparison of the resulting temperature field, 15 temperature sensors are installed inside the aluminum side wall, as well as inside the bulk fluid, equally distributed over the height. A schematic view of the experimental setup is shown in Figure 2. The principle of PLIF is based on the tem-

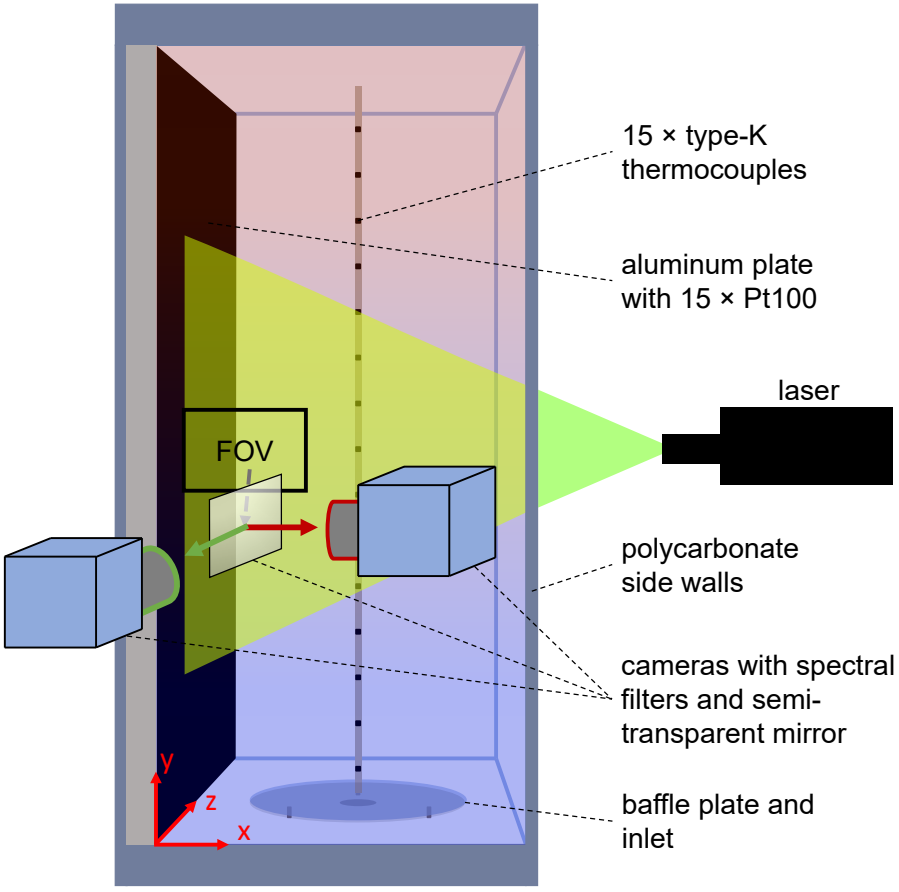

Figure 2. Scheme of the stratified thermal energy storage model experiment with the two-color planar laser induced fluorescence setup.

perature dependent fluorescence emission intensity of a fluorescent dye that is mixed into the investigated fluid. By illuminating a fluid plane with a laser light sheet and recording the fluorescence emission with a camera, the resulting intensity field can provide information about the temperature in the field of view. The fluorescence intensity I_f can be expressed as:

$$I_\mathrm{f} = I_0 \Phi c \epsilon, \tag{1}$$

where I_0 is the initial laser intensity, and Φ, c and ϵ are the quantum efficiency, molar concentration and molar absorptivity of the fluorescent dye (Coppeta & Rogers (1998)). Equation 1 shows that the fluorescence intensity directly depends on the laser intensity, which means that a constant and homogeneous laser light is essential for reliable measurements. Furthermore, a precise temperature calibration is required to convert the resulting fluorescence intensity field into a temperature field (Sakakibara & Adrian (1999)). By using two different fluorescent dyes instead of one and recording both emission intensities separately with one camera each and suitable spectral filters, a ratiometric approach can be applied, as expressed in Equation 2.

$$R = \frac{I_{\mathrm{f},1}}{I_{\mathrm{f},2}} = \frac{I_0 \Phi_1 c_1 \epsilon_1}{I_0 \Phi_2 c_2 \epsilon_2} \tag{2}$$

Here, R is the resulting intensity ratio of the fluorescence intensities of both dyes $I_{\mathrm{f},1}$ and $I_{\mathrm{f},2}$. The fraction on the right hand side indicates that R is independent of the initial laser intensity since it vanishes out. Assuming that the concentration of both dyes is constant in the fluid, the resulting intensity ratio only depends on the ratio of the quantum efficiencies and molar absorptivities. However, this 2C-PLIF approach is only valid as long as the fluorescence emission of both dyes shows linear behavior regarding small changes in concentration or incoming laser light. Furthermore, not only systematic measurement errors, caused by laser light fluctuation, can be eliminated (Coppeta & Rogers (1998)), but also the temperature sensitivity can be enhanced by specific dye combinations (Sutton et al. (2008); Chaze et al. (2016)). The latter can be achieved by choosing two different dyes with opposite temperature dependence of the fluorescence intensity. This is essential for resolving small local temperature gradients within the field of view. Hence, in this work, a combination of Fluorescein 27 (FL27, CAS: 80471-69-8, $\lambda_{\mathrm{peak,em}} = 521\,\mathrm{nm}$) with a molar concentration of $2.5 \times 10^{-7}\,\mathrm{mol\,L^{-1}}$ and Kiton Red (KR, CAS: 3520-42-1, $\lambda_{\mathrm{peak,em}} = 580\,\mathrm{nm}$) with a molar concentration of $2.5 \times 10^{-8}\,\mathrm{mol\,L^{-1}}$ is used. The low concentration is chosen to minimize possible absorption and reabsorption effects since the path of the laser light sheet and the optical path between light sheet and camera are rather large. By that, it is also ensured that the concentrations are far lower than the saturation level of the dyes at around $1.5 \times 10^{-6}\,\mathrm{mol\,L^{-1}}$.

For the investigations, the model experiment is filled from the bottom first with hot, dyed water at $60\,^{\circ}\mathrm{C}$, followed by cold, dyed water at $10\,^{\circ}\mathrm{C}$ to generate a stratification. Immediately after the filling process, a fluid plane at an optical depth of $z = 92\,\mathrm{mm}$ perpendicular to the aluminum side wall is illuminated by a laser light sheet with a modulated continuous wave Nd:YAG laser, exciting the fluorescent dyes. The emitted light is then split by a semi-transparent mirror and captured by two sCMOS cameras perpendicular to the laser light sheet. The 16-bit camera sensors have a resolution of $2560 \times 2160\,\mathrm{px}$, and are equipped with either $50\,\mathrm{mm}$ focal length objective lenses for the thermocline measurements or $100\,\mathrm{mm}$ focal length objective lenses for wall jet measurements in the hot region, which provide a spatial resolution of either $16.7\,\mathrm{px\,mm^{-1}}$ or $67.7\,\mathrm{px\,mm^{-1}}$, respectively. The first camera is equipped with a 550 / $20\,\mathrm{nm}$ band-pass filter to capture the spectrum of the FL27 emission, while the second camera is equipped with a 600 / $20\,\mathrm{nm}$ band-pass filter to

capture the emission of KR. As a consequence, both spectra are recorded separately with minimized spectral overlap. Figure 3 illustrates the resulting fluorescence emission spectrum of both fluorescent dyes, solved in water at the desired molar concentrations. Furthermore, the exciting laser wavelength and the spectra of both band-pass filters are shown. Due to the low concentration of KR, the captured fluorescence emission is lower compared to the emission of FL27. However, preliminary measurements have shown that this has an improving imapct on the resulting temperature sensitivity, and the measurements show that the captured signal is still sufficient for the 2C-PLIF measurements. For evaluation, the ratio of both captured intensity fields is calculated for

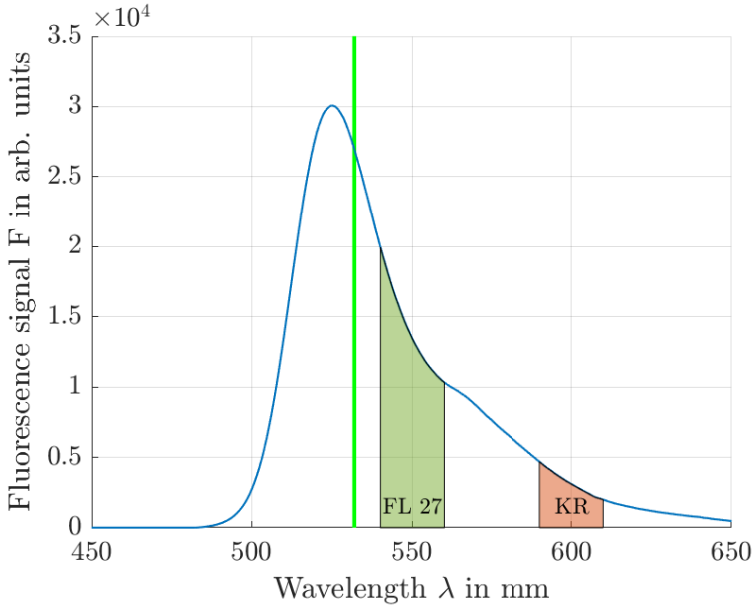

Figure 3. Fluorescence emission spectrum of FL27 and KR at a molar concentration of $2.5 \times 10^{-7}\,\mathrm{mol\,L^{-1}}$ and $2.5 \times 10^{-8}\,\mathrm{mol\,L^{-1}}$. Also indicated are the spectra of both band-pass filters, as well as the emission wavelength of the exciting laser.

every pixel with a 5×5 Gaussian smoothing filter applied, after dark image subtraction. Since the thermocline region vertically exceeds the field of view of both cameras, two separate 2C-PLIF measurements are performed at the lower and upper section of the thermocline region. While keeping similar experimental conditions, both data sets are combined in the post processing to fully resolve the thermocline region while keeping a high spatial resolution. In order to get information about the mixing process within the thermocline region over time, 1800 images are taken over the duration of $1\,\mathrm{h}$ at a measurement frequency of $0.5\,\mathrm{Hz}$. Furthermore, 1200 images are taken over the duration of $2\,\mathrm{min}$ at a measurement frequency of $10\,\mathrm{Hz}$ in the hot region of the storage directly at the wall in order to get information about the temperature distribution within the wall jet.
To ensure that the field of view is identical for both cameras, a geometric calibration is performed prior to the measurement. Therefore, a custom 2D-calibration target was positioned in the region of interest under identical experimental conditions. Additionally, an in-situ temperature calibration was performed prior to the measurements to relate the resulting intensity ratio of both flu-

orescent dyes to a known temperature. For that, the model experiment was filled with water at $60\,^{\circ}\mathrm{C}$ and then slowly cooled under constant stirring. At every $2\,^{\circ}\mathrm{C}$, 10 reference intensity ratios were recorded, averaged in the region of interest and calibrated to a reference Pt100 resistance thermometer with an uncertainty of $\sigma_{\mathrm{T,ref}} = \pm 0.1\,\mathrm{K}$. The reference thermometer was positioned in the field of view close behind the laser light sheet.

3. Results

3.1. Temperature calibration and sensitivity of the 2C-PLIF-system

In Figure 4, the resulting temperature dependence of the intensity ratio of the previously described 2C-PLIF setup is shown in the desired temperature range of $10\,^{\circ}\mathrm{C}$ to $60\,^{\circ}\mathrm{C}$. As visible, the intensity

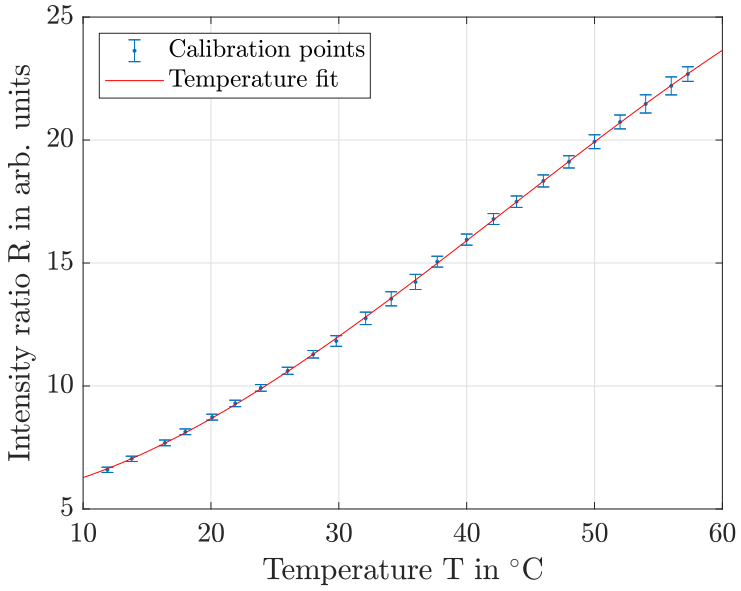

Figure 4. Intensity ratio R of both fluorescent dyes in dependence of the temperature T with the corresponding third order polynomial fit. The error bars indicate the standard deviation within the region of interest.

ratio was captured at 24 individual reference temperatures, equally distributed over the desired temperature range. The data points show a non-linear behavior. A third order polynomial fit was applied to the calibration points in order to obtain the temperature field from the measurement data. The fit has a maximum uncertainty within the $95\,\%$ confidence interval of $0.6\,^{\circ}\mathrm{C}$, based on the prediction bounds. Together with statistical and systematic uncertainties the of the camera sensors and the uncertainty of the reference thermometer (procedure similar to Kaaks et al. (2024) and Shi et al. (2021)), the overall temperature uncertainty is estimated to be in the order of $\Delta T = \pm 1.5\,^{\circ}\mathrm{C}$. In terms of the temperature sensitivity of the system, the highest sensitivity is obtained at $42\,^{\circ}\mathrm{C}$ with $S_{\mathrm{max}} \approx 6.1\,\%\,^{\circ}\mathrm{C}^{-1}$, with an averaged sensitivity of $S_{\mathrm{avg}} = 5.4\,\%$ over the

whole temperature range. These values are in agreement with the sensitivity values of similar systems (Sutton et al. (2008)). Regarding the measurements of very small temperature differences in the region of interest, especially the uncertainty of the camera noise is important. It provides information on the threshold, whether the temperature difference between a specific area in the field of view and surrounding fluid is detectable or not. To quantify this parameter, the standard deviation σ_{I} of a small section within the region of interest of an instantaneous intensity field at each reference temperature is analyzed. The small section of $50 \times 50\,\mathrm{px}$ is chosen to neglect possible systematic errors due to small temperature inhomogeneities or other image artifacts. Since the standard deviation typically increases with increasing intensity ratio due to higher signal levels, the highest value was found at $58\,^{\circ}\mathrm{C}$ with $\sigma_{\mathrm{stat}} = 0.18$, which corresponds to $0.33\,^{\circ}\mathrm{C}$. This means, in a $95\,\%$ confidence interval ($4\sigma_{\mathrm{stat}}$), local temperature differences are only detectable if they are larger than $1.32\,\mathrm{K}$ for single images. However, this value drastically decreases with averaging over multiple images. For example, with an average over 10 intensity fields, a temperature resolution of $T_{\mathrm{res}} = 0.41\,^{\circ}\mathrm{C}$ is achieved.

3.2. Thermocline measurements

With the performed temperature calibration, the 2C-PLIF-system can be applied and validated in the stratified TES model experiment. The temperature field of the thermocline region is shown in Figure 5 directly after the filling process (left) and after $60\,\mathrm{min}$ of stand-by time (right). The ther-

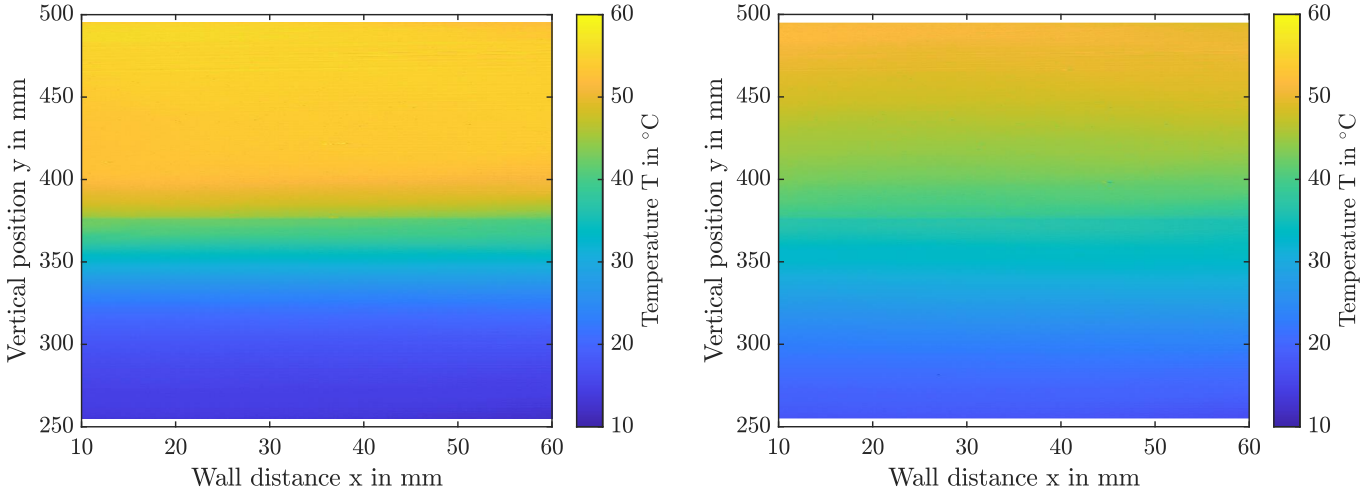

Figure 5. Temperature fields of the thermocline region of the stratified TES model experiment: left) directly after the filling process; right) after $60\,\mathrm{min}$ stand-by period. Both temperature fields are time-averaged over 5 images at a measurement frequency of $0.5\,\mathrm{Hz}$.

mal stratification of the fluid is clearly observable. Important to mention is the artifact in form of a vertical line at $y = 376\,\mathrm{mm}$, which is caused by the stitching of both data sets. The reason for

that might be a small shift in the vertical position of the thermocline region between both measurements. Additionally observable is that the thermocline region is increasing in size over time because of mixing, mainly caused by the near-wall convective flows and thermal diffusion.
To further analyze this effect, vertical temperature profiles at a wall distance of $x = 30\,\mathrm{mm}$ at $t = 0\,\mathrm{min}$, $30\,\mathrm{min}$ and $60\,\mathrm{min}$ after the filling process are shown in Figure 6. It is clearly visible that the temperature profiles flattening out over time, while the center of the thermocline region stays approximately at the same vertical position at $y_{\mathrm{center}} = 360\,\mathrm{mm}$. Furthermore, the change of the temperature profiles over time is stronger in the upper part of the thermocline region compared to the lower part, especially in the early stand-by phase from $0\,\mathrm{min}$ to $30\,\mathrm{min}$. Directly after the filling process, the upper thermocline part seems to have a distinct vertical position with a high vertical temperature gradient at $y \approx 400\,\mathrm{mm}$. Above this point, the temperature is almost constant. This indicates that the vertical separation of fluid layers with differing temperature is initially better in comparison to the lower thermocline region. For comparison, the temperature data of the thermo-

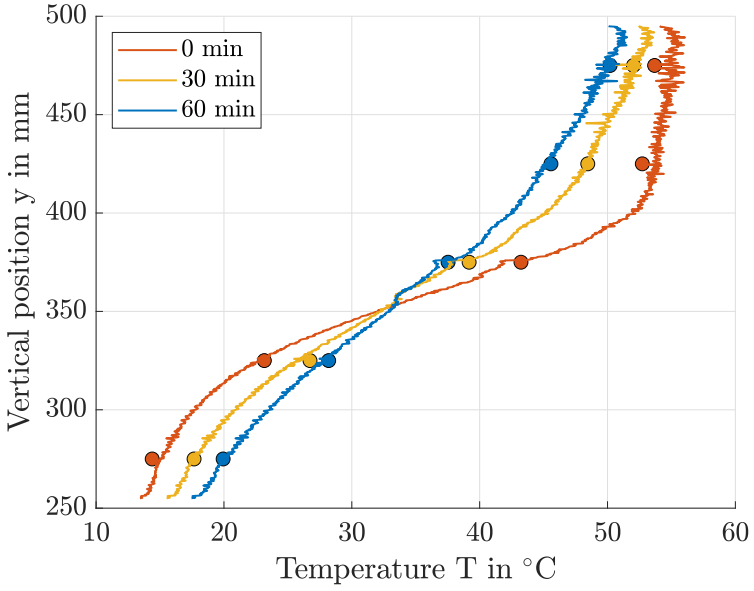

Figure 6. Vertical temperature profiles in the thermocline region at a wall distance of $x = 30\,\mathrm{mm}$ at 0, 30 and $60\,\mathrm{min}$ after the filling process. The intersection point of the profiles marks the vertical center of the thermocline region at $y_{\mathrm{center}} = 360\,\mathrm{mm}$. The dots indicate measured temperatures with thermocouples at the corresponding height and a wall distance of $x = 175\,\mathrm{mm}$.

couples in the fluid bulk within the thermocline region at a wall distance of $x = 175\,\mathrm{mm}$ are added to the graph. Despite some deviations in the upper region with a maximum difference of $0.9\,\mathrm{K}$, the overall values of the thermocouples are in good agreement with the measured temperature of the 2C-PLIF-system at the corresponding heights. Hence, this shows that the technique is suitable for evaluating the thermocline temperature distribution in such a system.

3.3. Near-wall hot region measurements

As explained in the introduction, one of the main points of this study is to quantify the influence of the wall jets on the mixing process. Hence, information on the temperature field within the vicinity of the wall is essential. Therefore, near-wall temperature field measurements in the hot region are performed. In Figure 7, a quasi-instantaneous temperature field of this region is shown, taken $5\,\mathrm{min}$ after the filling process and time-averaged over 5 images at a measurement frequency of $10\,\mathrm{Hz}$. The first thing to mention is that camera artifacts are visible in the resulting temperature

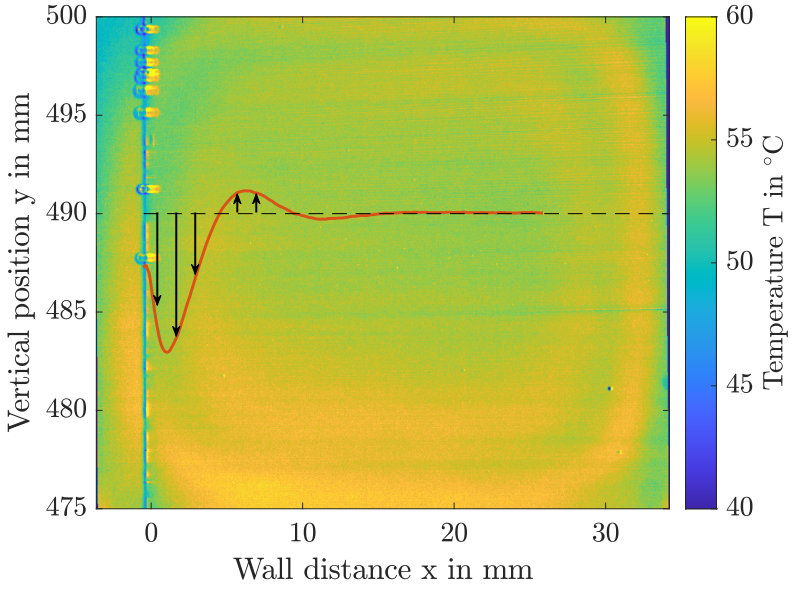

Figure 7. Quasi-instantaneous temperature field, averaged over 5 images at a measurement frequency of $10\,\mathrm{Hz}$ in the hot region, adjacent to the aluminum side wall. Also added is the local velocity profile of the downwards-moving wall jet at $y = 490\,\mathrm{mm}$ from previous PIV measurements by Otto & Cierpka (2021).

field. This is caused by inhomogeneous quantum efficiencies of the camera sensors, which is especially visible for small temperature ranges. For future studies, this effect can be eliminated by either performing a white image correction of both cameras in dependence of the exposure range, or by a pixel-based temperature calibration. However, both approaches are rather complex and will be topic of future evaluations.

Regarding the convective wall jets, a temperature difference compared to the surrounding bulk fluid is not detectable. In addition to the temperature field, the local velocity profile at $y = 490\,\mathrm{mm}$ from the previously performed PIV measurements by Otto & Cierpka (2021) is shown in order to put the dimensions into context. Based on the graph, it can be concluded that the wall jet temperature is very similar to the surrounding fluid and below $1.2\,^{\circ}\mathrm{C}$ for an instantaneous temperature field. However, based on the temperature sensor measurements inside the aluminum wall and inside the fluid bulk, a temperature difference of up to $3\,^{\circ}\mathrm{C}$ is present between wall and fluid. Since this temperature difference is not observable in the measurement results, it is expected that

the thermal boundary layer adjacent to the wall is very small. This is also in agreement with the theory, since the Prandtl number is ≈ 4 for water in the observed region, which means that the thermal boundary layer in general is four times smaller compared to the velocity boundary layer. As a consequence, the thermal boundary layer is not resolvable with the current 2C-PLIF setup due to limited spatial, and especially temperature resolution. Nevertheless, with simultaneously performed PIV measurements in future investigations, it is possible to quantify the influence of the convective wall jets on the mixing process in the stratified TES model experiment, especially in the thermocline region with high temperature gradients.

4. Conclusion

This paper presents temperature field measurements inside a stratified thermal energy storage (TES) model experiment based on two-color planar laser induced fluorescence (2C-PLIF). The results show that the temperature distribution within the thermocline region can be measured sufficiently in order to get information on the increase of the thermocline thickness over time. Furthermore, information about the in-situ calibration process and the resulting temperature fit is provided. By performing two independent measurements of different vertical positions within the thermocline region and subsequent stichting of the resulting temperature fields, it was possible to obtain a larger field of view while keeping a high spatial resolution. The resulting LIF temperatures were also compared with temperature data of vertically distributed thermocouples within the bulk region, which only show slight deviations that are within the measurement accuracy of $1.5\,^{\circ}\mathrm{C}$. However, further studies of the near-wall region in the hot fluid layer have shown that the measurement of the thermal boundary layer adjacent to the wall is limited by the temperature resolution of the measurement system. A temperature difference between the wall jet and surrounding fluid was not observable. Additionally, camera artifacts, caused by differing quantum efficiencies of the camera sensors, impede precise temperature measurements with low thermal gradients within the field of view. However, this can be resolved in future studies by a white image correction and a pixel-wise temperature calibration. In summary, the implemented 2C-PLIF method provides sufficient information on the temperature field of the wall jet and the thermocline region. This is of special interest for future studies, which aim to determine local heat fluxes in combination with simultaneous PIV measurements.

Acknowledgements

The authors would like to acknowledge Nicolas Stark and Alexander Thieme for their assistance in implementing the measurements, setting up the experiments, and their valuable discussions. Furthermore, the authors greatfully acknowledge financial support from the German Research Foundation within the priority programme 2403 'Carnot Batteries' under grant no. 525893212.

Nomenclature

ΔT	Temperature uncertainty [$^{\circ}\mathrm{C}$]
ϵ	Molar absorptivity of fluorescent dye [$\mathrm{m^2\,mol^{-1}}$]
F	Fluorescence signal [-]
I_0	Initial laser intensity [$\mathrm{W\,m^{-2}}$]
I_f	Fluorescence intensity [$\mathrm{W\,m^{-3}}$]
λ_f	Thermal conductivity of the storage fluid [nm]
λ_w	Thermal conductivity of the storage tank wall [nm]
$\lambda_\mathrm{peak,em}$	Wavelength of the emission spectrum peak of the fluorescent dye [nm]
Φ	Quantum efficiency of fluorescent dye [-]
R	Fluorescence intensity ratio [-]
S_max	Maximum temperature sensitivity [$\%\,^{\circ}\mathrm{C^{-1}}$]
S_avg	Average temperature sensitivity [$\%\,^{\circ}\mathrm{C^{-1}}$]
$\sigma_\mathrm{T,ref}$	Uncertainty of the reference thermometer [$^{\circ}\mathrm{C}$]
σ_stat	Spatial standard deviation of the instantaneous intensity ratio field [-]
T	Temperature [$^{\circ}\mathrm{C}$]
T_{res}	Temperature resolution [$^{\circ}\mathrm{C}$]
x	Wall distance [mm]
y	Vertical position [mm]
z	Optical depth [mm]

References

Chaze, W., Caballina, O., Castanet, G., & Lemoine, F. (2016). The saturation of the fluorescence and its consequences for laser-induced fluorescence thermometry in liquid flows. *Experiments in Fluids*, *57*, 58.

Coppeta, J., & Rogers, C. (1998). Dual emission laser induced fluorescence for direct planar scalar behavior measurements. *Experiments in Fluids*, *25*, 1–15.

Dumont, O., Frate, G. F., Pillai, A., Lecompte, S., de paepe, M., & Lemort, V. (2020). Carnot battery technology: A state-of-the-art review. *Journal of Energy Storage*, *32*, 101756.

Kaaks, B. J., Couweleers, S., Lathouwers, D., Kloosterman, J.-L., & Rohde, M. (2024). Non-intrusive temperature measurements for transient freezing in laminar internal flow using laser induced fluorescence. *Experimental Thermal and Fluid Science*, *155*, 111184.

Otto, H., & Cierpka, C. (2021). Influence of thermal stratification on vertical natural convection—experimental investigations on the example of thermal energy storage systems. *Physics of Fluids*, *33*, 083614.

Otto, H., Naumann, C., Odenthal, C., & Cierpka, C. (2023). Unsteady inherent convective mixing in thermal-energy-storage systems during standby periods. *PRX Energy*, *2*, 043001.

Sakakibara, J., & Adrian, R. J. (1999). Whole field measurement of temperature in water using two-color laser induced fluorescence. *Experiments in Fluids*, *26*, 7–15.

Shi, H., Di Micheli Raimondi, N., Cid, E., Cabassud, M., & Gourdon, C. (2021). Temperature field acquisition by planar laser induced fluorescence using the two-color/two-dye technique for liquid flows in a millimetric zigzag channel. *Chemical Engineering Journal*, *426*, 131460.

Sutton, J. A., Fisher, B. T., & Fleming, J. W. (2008). A laser-induced fluorescence measurement for aqueous fluid flows with improved temperature sensitivity. *Experiments in Fluids*, *45*, 869–881.